Metamorphic diamonds in a garnet megacryst from the Edough Massif (northeastern Algeria). Recognition and geodynamic consequences

Renaud Caby, Olivier Bruguier, Laure Fernandez, Dalila Hammor, Delphine Bosch, Mehdi Mechati, Rabah Laouar, Aziouz Ouabadi, Nachida Abdallah, Chantal Douchet

Metamorphic diamonds in a garnet megacryst from the Edough Massif (northeastern Algeria). Recognition and geodynamic consequences

Renaud Caby [a], Olivier Bruguier [a,*], Laure Fernandez [a], Dalila Hammor [b], Delphine Bosch [a], Mehdi Mechati [b], Rabah Laouar [b], Aziouz Ouabadi [c], Nachida Abdallah [c], Chantal Douchet [a]

[a] Géosciences Montpellier, Université de Montpellier II, CNRS-UMR 5243, Place E. Bataillon, 34095 Montpellier cedex 5, France
[b] Laboratoire de Recherche Géologie, Faculté des Sciences de la Terre, Université Badji Mokhtar, BP.12, Annaba 23000, Algeria
[c] Université des Sciences et Techniques Houari Boumedienne, Bab Ezzouar, Laboratoire de Géodynamique, Géologie de l'Ingénieur et Planétologie, (LGGIP/FSTGAT/USTHB), Alger, Algeria

Keywords:
Metamorphic diamond
Ultrahigh pressure
Edough Massif
Algerian basin
Western Mediterranean

a b s t r a c t

We report for the first time the discovery of diamond inclusions (5–30 μm in size), identified by Raman spectroscopy and the characteristic sharp band at 1332 cm^{-1} for crystalline diamond, in a garnet megacryst (≥5 cm) from the Edough Massif (NE Algeria). The garnet is adjacent to actinolite and ultramafic boudins and slices of marbles that are inserted within a major mylonite–ultramylonite band. This tectonic contact sharply delineates the Kef Lakhal oceanic unit from the granite-gneiss core below. The host garnet is almandine-dominant and is rich in exsolution of acicular rutile needles. Major and trace elements show a gradual but significant zonation from core to rim, and a sharp increase in grossular component in the rim. Trace element analyses of prismatic rutile inclusions up to 300 μm in size indicate that the host metamorphic rock was a mafic protolith of MORB affinity. The Zr-in-rutile thermometry indicates a temperature range of 724–778 °C that we relate to rutile growth, either during prograde metamorphism or under peak UHP metamorphic conditions of ≥3.6 GPa that were reached during subduction of the UHP-rock precursors. We suggest that the mafic protolith originates from the subducted retreating Calabrian branch of the Tethyan slab, that broke or tore, and which fragments were dragged upward and thrust onto the North African margin along with the Kef Lakhal unit, shortly followed by formation of the Edough dome and opening of the Algerian basin.

1. Introduction

Ultrahigh-pressure (UHP) metamorphic terrains are known from several orogenic belts and diamond-bearing metamorphic rocks, indicating pressure conditions ≥3.0–3.5 GPa, and have been discovered in more than 20 localities worldwide. These occurrences are known in the Early Paleozoic, Variscan, Mesozoic and Alpine orogens (Dobrzhinetskaya, 2012; Gilotti, 2013; Liou et al., 2009; Shertl and O'Brien, 2013). The geodynamic settings that allow the rocks to undergo UHP metamorphic conditions require subduction of material, either continental or oceanic, at mantle depth. The recognition and the study of UHP material thus bring important information on the deep subduction of the oceanic lithosphere (and its sedimentary cover) and of the attached continental crust, on the recycling of continental materials through subduction, and on the exhumation mechanisms and return to the surface of these rocks. For example, it has been argued that diamond-bearing metamorphic rocks of continental origin represent crustal slices extruded from a subduction channel and tectonically inserted between lower pressure units. The close association of garnet peridotites with UHP granulites, such as in the Rif and Betic Cordillera (Ruiz-Cruz et al., 2011 and references therein) suggests that the peridotites were interdigitated within subducted continental crust rather than being tectonically emplaced at shallow crustal levels. In addition, the recent discovery of microdiamonds and coesite in staurolite–andalusite schists from the Betic Cordillera, far from mantle peridotites, suggests that micrometer-sized diamond is the only preserved record of prograde UHP conditions having affected sediments in a subduction context (Ruiz-Cruz and Sanz de Galdeano, 2013a). In that case, the critical UHP mineral assemblages were totally erased (except coesite and diamond) by later lower pressure recrystallization.

This paper reports for the first time in NE Algeria, the discovery of metamorphic diamonds included in a garnet megacryst. This discovery complements and broadens the spectrum of diamond-bearing rocks identified in the Western peri-Mediterranean area. We first review the geological framework of this massif, then describe the occurrence of the diamond inclusions and evaluate the possible geodynamic consequences of this finding for the different models describing the evolution of the Western Mediterranean and the Cenozoic opening of (oceanic) basins in a broadly compressive context dominated by the northward motion of Africa and the eastward retreat of the Calabrian branch of the Tethyan slab.

2. Geological framework of the Maghrebides in Algeria

The geology of the Maghrebides has been extensively studied since more than 50 years and has been synthesized in classical papers (e.g. Bouillin et al., 1986; Frizon de Lamotte et al., 2000; Michard, 2006 and references therein). The internal zones of the Maghrebides include the Kabylian crystalline Massifs (Lesser and Greater Kabylia; Fig. 1a) that were part of the Variscan belt of Western Europe and have been capped by the Mesozoic sedimentary cover. In Greater Kabylia, this basement comprises Paleozoic sediments, schists, gneisses, anatexites and late Variscan granites. The high-temperature metamorphism coeval with anatexis has been dated as Lower Permian (Hammor et al., 2006; Peucat et al., 1996). Tectono-metamorphic events also took place during the Mesozoic period according to $^{40}Ar/^{39}Ar$ ages of 128 Ma on white micas (Cheilletz et al., 1999). Formation of metamorphic cores, exhumation of the middle and lower crustal units and unroofing of the non-metamorphic upper units took place in the Miocene, during the major syn- to late-metamorphic extensional event (Monié et al., 1988). Miocene tectono-metamorphic overprint of deep greenschist to amphibolite facies conditions was sufficiently intense to be responsible for new mica generation (Monié et al., 1988), for the replacement of andalusite from the thermal aureoles of Variscan plutons by kyanite (Saadallah and Caby, 1996) and for the thorough reset of the Rb–Sr and Ar/Ar systems of Variscan micas (Hammor et al., 2006; Peucat et al., 1996). These crystalline units were exhumed and eroded prior to the deposition of the unconformable molassic sediments (Kabylian Oligo-Miocene), and later emplaced over the Numidian nappe during the Burdigalian (21.5–16.3 Ma). The Lesser Kabylia massif is lithologically similar to Greater Kabylia but it is involved in a 2 to 5 km thick crystalline nappe emplaced southward above the Tellian units. The Tellian nappes represent the Mesozoic African passive margin, with discrete Jurassic basaltic volcanism, that either escaped Alpine metamorphism or was affected by very low- to low-greenschist facies metamorphism (Mahdjoub et al., 1997; Michard et al., 2006). This short review highlights the alternation of compressional and extensional stages recognized in the Maghrebides. The Edough Massif, that is dealt within this study, emerges below the Tellian nappes and has therefore been considered as part of the African crust since Vila (1970).

3. Tectonometamorphic characters of the Edough crystalline units

The Edough Massif displays a dome geometry and shares the classical tectonic features of metamorphic core complexes (Block and Royden, 1990; Brun and Van Den Driessche, 1994; Davis, 1987; Lister and Davis, 1989). A uniform W–NW sense of shear generated in an extensional regime has been recognized in all units (Brunel et al., 1988; Caby and Hammor, 1992; Caby et al., 2001). The massif exposes granite-gneisses and diatexites in its core (Fig. 1b) overlain by high-

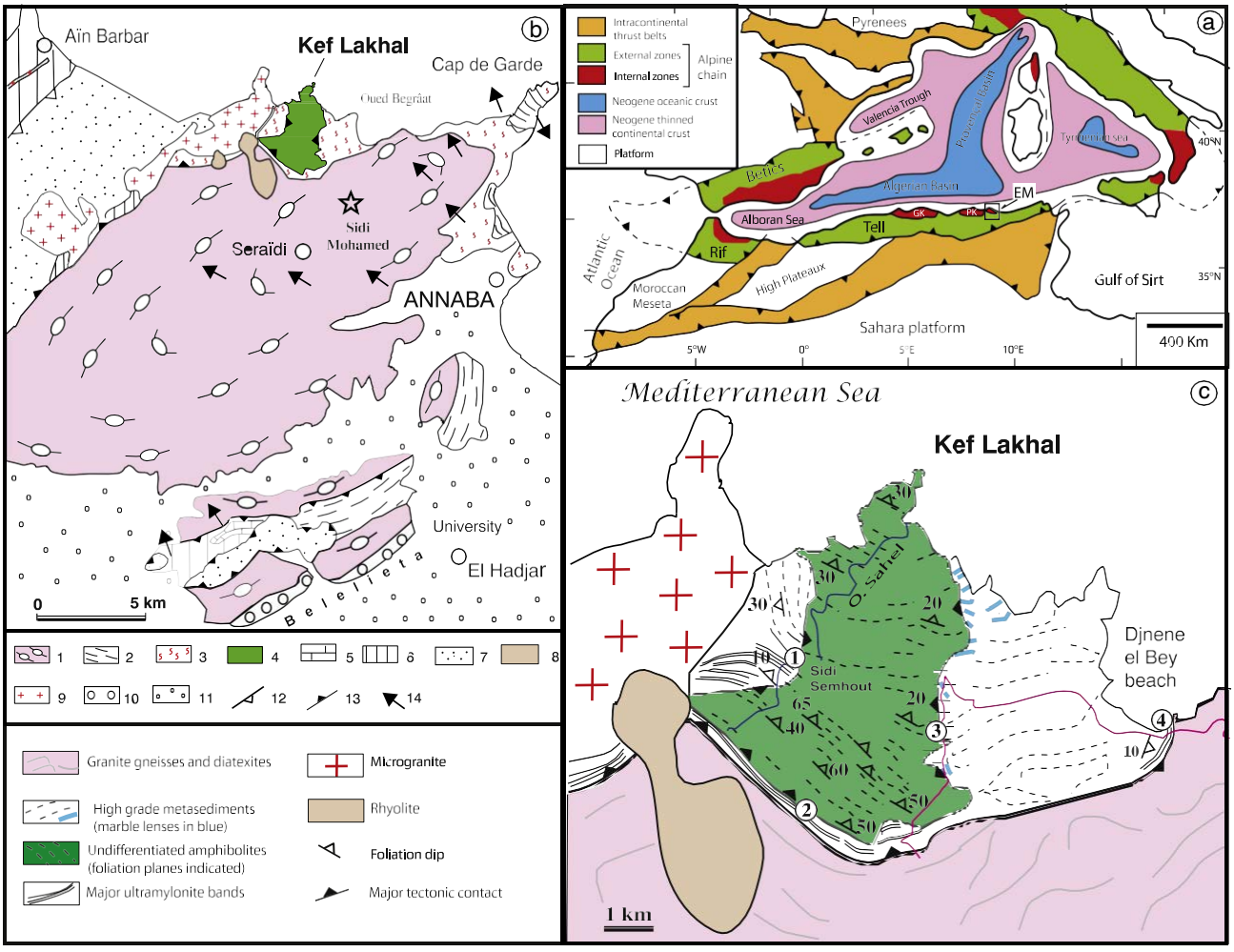

Fig. 1. a) Tectonic framework of the Western Mediterranean basin showing the location of the Maghrebides (modified after Frizon de Lamotte et al., 2000); b) schematic geological sketch map of the Edough Massif (after Caby et al., 2001). 1—granite-gneisses; 2—micaschists; 3—high temperature metamorphic rocks; 4—undifferentiated mafic and ultramafic rocks; 5—Jurassic marbles; 6—cretaceous marls and flysch; 7—Numidian nappe; 8—rhyolite; 9—microgranite; 10—Pliocene sediments; 11—Quaternary cover; 12—thrust; 13—major normal fault; shear criteria; c) enlargement showing the Kef Lakhal area. Circles 1 to 4 refer to localities mentioned in the text.

grade metasedimentary units and, on top, the Kef Lakhal (La Voile Noire) metabasic complex.

3.1. Granite-gneisses and diatexites

The core of the massif mainly consists of sheeted granite-gneisses, metaaplites and diatexites. Sheets of tourmaline-bearing leucogranite and aluminous aplites intrude the Annaba metapelites of assumed Paleozoic age. A hectometer-sized elliptical body of ultramafic rock, the "Sidi Mohamed peridotite" (see Fig. 1b), is inserted in diatexites (Bossière et al., 1976; Hadj-Zobir and Oberhansli, 2013). The peridotites represent parts of the sub-continental lithospheric mantle (Bosch et al., 2014) that was incorporated in the crustal roots of the Edough Massif at c. 18 Ma, during the early stages of opening of the Algerian basin (Bruguier et al., 2009). The contact with the enclosing diatexite on its southeast side consists of a 5 m thick band of two-pyroxene-actinolite ± garnet phlogopitite sharply cut by veins of garnet metagabbro. The primary mineral assemblage preserved in the thicker veins of the garnet metagabbro is eclogitic (omphacitic clinopyroxene (Jd25), garnet, quartz, zoisite and prismatic rutile), that according to Caby et al. (2001), represents conditions of T = 730–750 °C and P = 12–13 kbar.

3.2. High grade metamorphic unit

High-grade metamorphic rocks from the northwestern part of the massif are exposed between Djnene el Bey beach and Kef Lakhal (Fig. 1c). These encompass anatectic metapelites, quartzites, calc-silicate gneisses and a marble unit. Complex metamorphic assemblages from metapelites and calc-silicate rocks are garnet-rich. Most metapelites show evidence for a diversely overprinted early high-pressure metamorphic event. Aluminous metapelites contain primary phengitic mica (always with Si ≤3.2 pfu.), kyanite, garnet and rutile, and lack primary biotite. Near isothermal decompression is best portrayed in most metapelites by andalusite + fibrolite replacing kyanite assemblages, by exsolution of biotite from white mica and by biotite replacing garnet (Caby et al., 2001). In contrast, some garnet–kyanite-rich peraluminous Fe–Mg metapelites of restitic character suffered weak retrogression. Garnet cores (alm65 pyr09 grs25 spe1) from such rocks, crowded by acicular zoisite and rutile inclusions, indicate fossilized medium temperature, high-pressure conditions in contrast with the rims (alm45 pyr37 grs17 sp1) related to growth at peak temperature. Pyrope-rich garnets (pyr47 alm44 grs09 spe1) characterize some diatexites in the same area. Metamorphic conditions of T = 700–750 °C and P = 12–14 kbar have been calculated by Caby et al. (2001) for the early metamorphic conditions.

3.3. Kef Lakhal (La Voile Noire) amphibolite complex

The Kef Lakhal complex, about 1000 m thick, consists of layered amphibolites, in which most amphiboles are pargasitic hornblendes of metamorphic origin (Ahmed-Said and Leake, 1992, 1997). Igneous layering, represented by variable abundances of plagioclase and ferro-magnesian minerals, suggests that the protoliths were layered metagabbros. Major trace elements and Pb–Sr–Nd isotopes argue for a Depleted Mantle origin and a back-arc setting, implying that the complex was obducted onto the North African margin (Bosch et al., 2014). Garnet-bearing amphibolites are more abundant toward the base of the complex that also includes boudins of garnet–plagioclase pyroxenites with occasional coronitic microstructures, but no evidence of retrogressed eclogites. The replacement of metamorphic amphiboles by clinopyroxene is frequently observed in thin sections and dehydration melting of amphibolites under high-pressure conditions is evidenced by the early generation of plagioclase–clinopyroxene- and garnet–clinopyroxene–quartz–rutile leucosomes. Pressure–temperature estimates calculated by Caby et al. (2001) for the early HP stage are T = 770–835 °C and P = 10–13 kbar. A second generation of garnet-free, amphibole–plagioclase–titanite ± quartz leucosomes indicates up to 20 vol.% of partial melting at lower pressure. Upward in the section, strongly banded and finer grained amphibolites display occasionally isoclinal folding at cm- dm- scale. Most of these rocks represent syn-metamorphic mylonites. Diffuse epidote–quartz pods and bands, occasionally up to 20 vol.% in thin section, emphasize the selective replacement of calcic plagioclase by epidote. Others bands oblique to the foliation may represent deformed hydrothermal veins. The top of the complex comprises fine-grained mylonitic epidote–amphibolites probably derived from dolerite. Other epidote- and carbonate-enriched layers are possibly derived from epiclastites or metatufs.

3.4. Kinematics and major mylonite–ultramylonite bands

Shear-sense indicators observed in the mylonites and in the country rocks of the Edough Massif indicate top-to-the NW displacements (Brunel et al., 1988; Caby and Hammor, 1992; Gleizes et al., 1988). Such kinematics is opposite to the S-SE compressive kinematics of early Oligocene age observed in the Tellian units and in the basement units of Lesser Kabylia (Mahdjoub et al., 1997). Caby and Hammor (1992) suggested that the kinematics in the Edough Massif are of Miocene age and proposed that all tectonic contacts represent late-metamorphic extensional faults related to the dome development, as reported from other well studied metamorphic core complexes (e.g. Gautier and Brun, 1994; Lister and Davis, 1989).

The main mylonite zone that delineates the oceanic units of the Kef Lakhal complex and the granite-gneisses from the dome below shows only evidences for top-to-the NW-directed normal shear. Deformation gradients show that quartzo-feldspathic mylonites derived from the underlying coarse-grained gneisses, granitoids and metasedimentary units of the footwall. Ultramylonites of pelitic origin are depicted by spherical clasts of minute garnet set up in a very fine-grained (≤50 μm) banded biotite-rich ± fibrolitic matrix. Such high-temperature ultramylonites are well exposed 500 m southeast of Sidi Semhout along Oued Sahel (Fig. 1c, locality 1), where they contain boudins, lenses and spherical pseudo-pebbles (cm to m size) of various types of amphibolites from the overlying Kef Lakhal complex. At locality 2 (Fig. 1c), along the Kef Lakhal ridge, the same mylonite band (c. 50 m thick) exposes lenses of marble, quartzite and boudins of ultramafic rocks among which coarse-grained dunite and actinolite pods occur. Garnet megacrysts (5 to 10 cm across, including the studied sample ED128) are apparently hosted by actinolitite but can only be sampled from the saprolitic soil. The same band depicted by boudins of various types of carbonated ultramafics (including spinel peridotite and dunite) can be observed in the road cuts (locality 3) over some 200 m. At locality 4, along the shore, another mylonite/ultramylonite band about 15 m thick is exposed but it sharply delimits the high-grade metasediments of the footwall from granite-gneisses in the hanging wall. The boudins dispersed in this band comprise several types of coarse-grained calc-silicate gneiss inserted in various mylonitic metapelites among which garnet-, white mica- and kyanite-rich types can be differentiated. Meter-sized boudins of amphibolite, calc-silicate gneiss and one lens of massive diopsidite with centimetric wollastonite prisms are concentrated within a phlogopite-rich mylonitic horizon a few meters thick that was affected by a late gouge network. Numerous decimeter-sized boudins of carbonated ultramafite, including dunite and garnet megacrysts fringed by a plagioclase corona, are scattered within this mylonite band. This outcrop also exposes one spectacular nearly spherical boudin of coarse-grained peridotite c. 4 m across, cut by talc veins (Fig. 2A). The peridotite displays subhedral orthopyroxene (1–3 cm), clinopyroxene and almost fully serpentinized olivine grains, set up in a matrix (c. 20 vol.%) of talc, brucite and actinolite. Other decimeter scale mylonite/ultramylonite bands cutting at low angles of the foliation of anatectic metapelites have also been observed. The recognition of

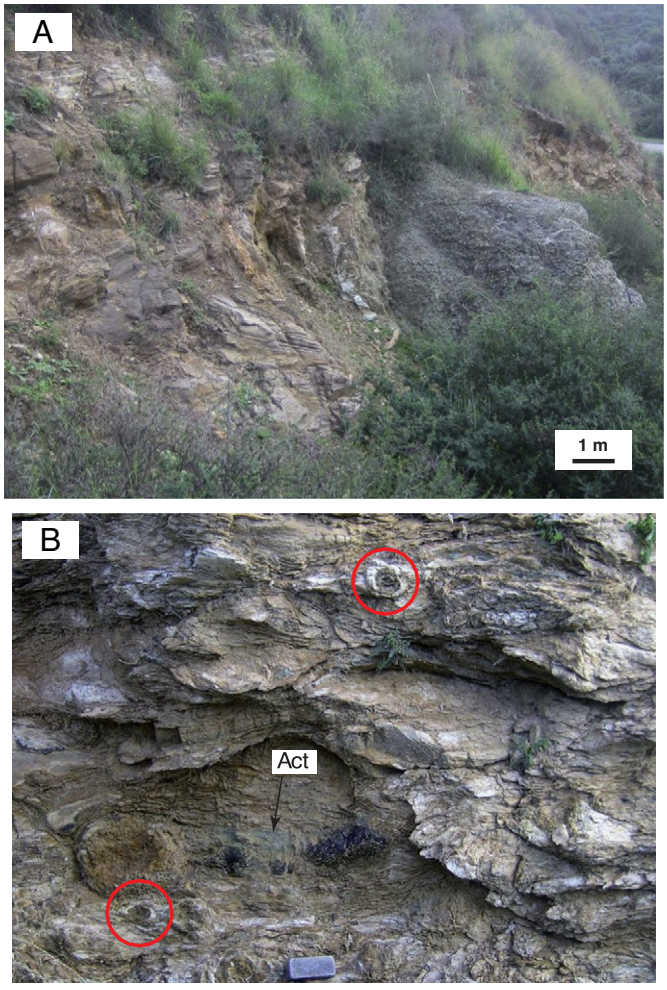

Fig. 2. Photographs of outcrops described in the text. (A) Boudin of coarse-grained peridotite enclosed in the mylonite band of locality 4. (B) View of the weathered mylonitic rocks from locality 4. Blackish and brown boudins are ultramafic rocks dispersed in a tectonic mélange of mylonitic metapelites and actinolite lenses (in green). Garnet megacrysts displaying a plagioclase halo are encircled in red.

several mylonite/ultramylonite bands allows considering that major syn-to late-metamorphic tectonic contacts are present in the pile of the Edough Massif.

4. Sample description

The diamond-bearing garnet megacryst ED128 was collected at locality 2 (see Fig. 1c) in the main mylonite band c. 50 m thick that separates the overlying Kef Lakhal complex from the granite-gneisses below. Several fragments of garnet megacrysts, up to 5 cm across, have been collected from the poorly exposed contact zone that only displays coarse-grained actinolitite and altered ultramafic boudins adjacent to marble slices. Although the exact nature of the protolith of the ED128 megacryst cannot be ascertain with confidence, Fig. 2B gives a possible equivalent for the context of ED128. The garnet megacryst ED128 displays zones with variable amounts of inclusions, from inclusion-free to inclusion-rich domains (Fig. 3A, B). Most of the garnet is rich in a dense network of rutile needles (μm size) displaying a crystallographic orientation throughout the megacryst (Fig. 3C, D), although few domains are apparently free of such rutile needles. In addition, the megacryst contains numerous, randomly oriented prismatic rutile inclusions, tens to hundred of μm in size (Fig. 3E, F, J). These rutiles occur in bands while domains free of inclusions are also observed. The prismatic rutiles are interpreted as inclusions formed and included in garnet during its growth, while the small, acicular, oriented rutile needles are exsolutions from the garnet megacryst. The bands with variable abundance of TiO_2 exsolutions are reminiscent of growth zoning. A dense oriented rutile exsolution network inside a sodic garnet has been taken as evidence for a majoritic garnet precursor (Mposkos and Kostopoulos, 2001), although this has been questioned by Chopin (2003), who indicates that only OPX exsolutions are symptomatic of a majoritic precursor. Microdiamonds, a few tens per cm^2, are only observed within the rutile-rich bands. This mineral ranges in size from 5 to 30 μm and has been first identified on polished thick sections observed under transmitted and reflected light by its optical characters (cuboid and octahedrons, positive topography, see Fig. 3G, H, I, J) and then by Raman spectroscopy through their characteristic intense sharp band at 1332 cm^{-1} (Fig. 3K). The other identified monomineral inclusions in the garnet are minute euhedral zircon (≤ 30 μm) often in contact or close to prismatic rutile (Fig. 3L, M), ilmenite either as individual grains or as lamellae in prismatic rutile, plagioclase An25-27 Or0.50, acicular Jd-poor pyroxene (Na_2O ≤ 1.58), staurolite and kyanite. Multiphase inclusions were also detected and are constituted by isomorphic (Fig. 3M) or anhedral shaped inclusions. Minerals in the multiphase inclusions include apatite, kyanite and amphibole.

5. Analytical technique

Raman spectroscopy was carried out at the University of Montpellier II using a Dilor RT30 spectrometer. Major element analyses of minerals were performed using a Cameca SX100 equipment at the University of Montpellier II, using an acceleration voltage of 15 kV, a beam current of 20 nA, and a beam diameter of 1 μm. The SEM study was carried out using an Environmental Scanning Electron Microscope FEI at the University of Montpellier II, using an acceleration voltage of 15 kV. Trace element analyses of minerals were performed in situ by laser ablation ICP-MS on a Element XR single collector ICP-MS coupled to a 193 nm Compex 102 Excimer laser. Spot sizes of 51 μm were used for garnet and rutile, along with an energy density of 10 J/cm^2 and a 6 Hz frequency. Each analysis included a background acquisition of 120 s, followed by 60 s data acquisition of the sample. Data were processed using the Glitter software (Gemoc). Element concentrations were calibrated against the NIST612 certified reference material, using the values of Pearce et al. (1997). Si^{29} and Ti^{49} were used as internal standards for garnet and rutile respectively, based on their SiO_2 and TiO_2 content as measured by electron microprobe.

6. Results

The chemical data from the garnet megacryst ED128 and its prismatic rutile inclusions are reported in Table 1 (electron microprobe) and Table 2 (laser ablation).

6.1. Garnet

The garnet megacryst ED128 has been analyzed for major elements at four locations across the crystal (see Fig. 4A for location). EPMA analyses reveal a variation between the inner and outer part of the megacryst (see Table 1). The garnet shows a gradual zoning with a notable increase in pyrope (from 31.3 to 34.8 mol%) and a decrease in almandine (from 55.7 to 52.8 mol%) and spessartine (from 2.7 to 1.4 mol%) toward the outer part. The grossular content shows a trend characterized by a slightly decreasing content toward the outer part (from 10.7 to 9.8 mol%) followed by an abrupt increase in the outermost part (10.9 mol%). These compositional trends are broadly similar to prograde growth-zoning patterns of garnets from different HP and

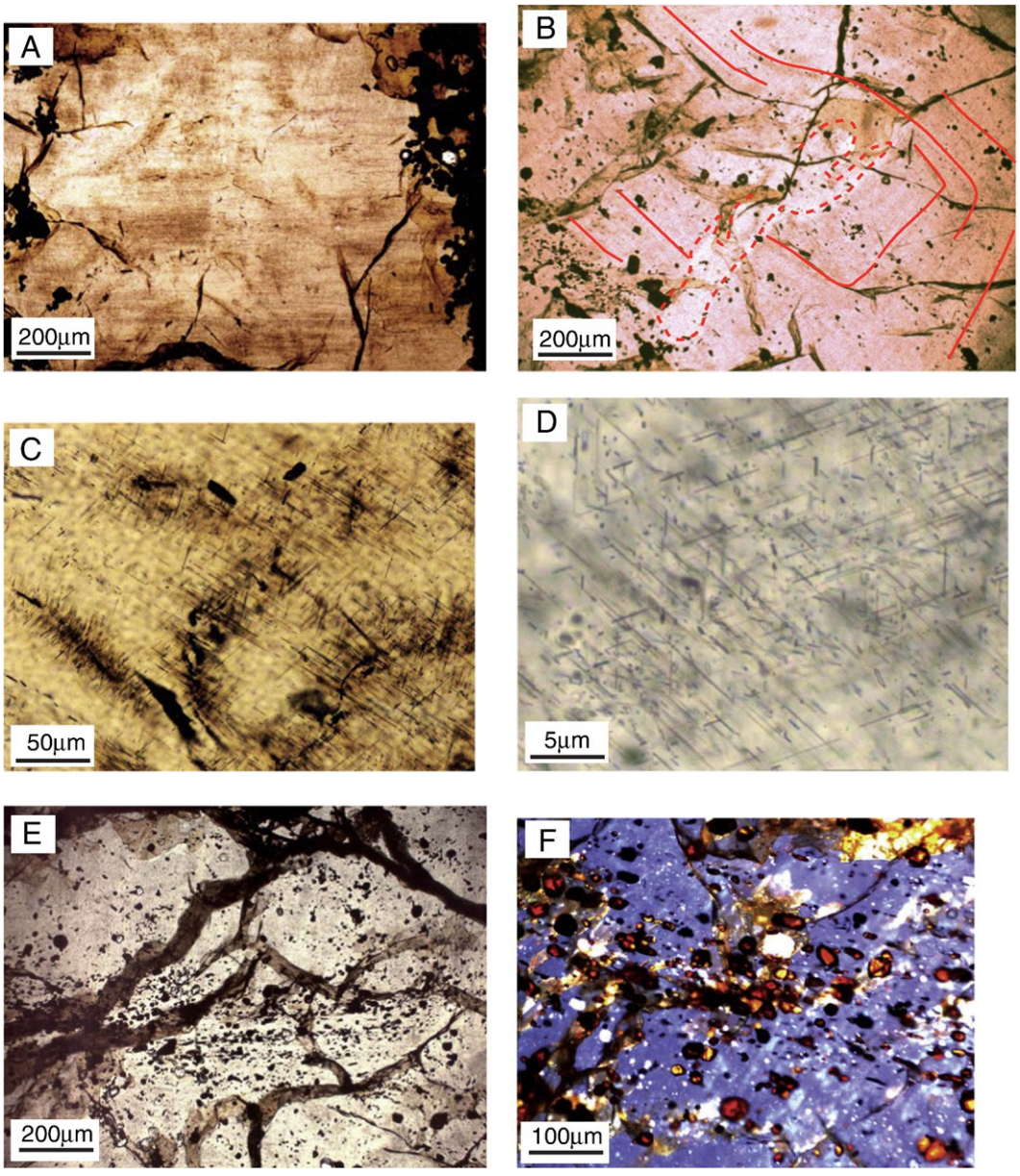

Fig. 3. Selected microphotographs of garnet megacryst ED128 and its inclusions. (A) Banding reflecting variable abundances of rutile exsolutions. The clear domains nearly free of inclusions contain up to 0.2 wt.% of TiO_2. (B) Detail showing the variable abundance of rutile needle exsolutions suggestive of growth zoning (enhanced in red); note the white inclusion-free domains (dotted). (C, D) Details showing domains with a dense network of rutile needles. Note the triangular pattern visible in (D). (E) Banding aspect of the prismatic rutile inclusions interpreted as a folded early foliation (plane light). (F) Enlarged part of (E) showing a domain with ≥5 vol.% of rutile inclusions, some of them displaying a platy fabric (plane light). (G) Detail of a string of inclusions (plane light). (H, I) Cuboids of diamond (plane light). (J) Rutile and diamond inclusions (reflected light). (K) Raman spectra of the diamond inclusion shown in J, showing the sharp band at 1332 cm^{-1}. (L) SEM and natural light images of a prismatic euhedral rutile grain. The bright lamellae is ilmenite exsolution. (M) Isomorphic polyphase inclusion containing kyanite, apatite and amphibole. Symbols after Kretz (1983).

UHP belts worldwide (Konrad-Schmolke et al., 2008a). The chemical composition of ED128 megacryst is consistent with a classical substitution where phosphorus enters the garnet structure by the coupled substitution $Na^{+} + P^{5+} \rightarrow Si^{4+} + Ca^{2+}$ (Thompson, 1975). This is supported by the negative correlation observed in the inner part of the megacryst between Na on one hand and Si or Ca on the other hand (Fig. 4B and C). Experimental data using ultramafic composition (Konzett et al., 2012) indicates that the phosphorus solubility in garnet is pressure dependent with P_2O_5 content around 0.07% at 2.5 GPa (900 °C) and 0.26% at 4 GPa (1000 °C). The inner part of ED128 megacryst yields a phosphorus content in the range from 0.073 to 0.128% (see Table 1), suggesting that most of the megacryst grew at pressure above 2.5 GPa.

Trace element patterns measured at different locations yield chondrite-normalized REE patterns (Fig. 5) characterized by low LREE content and flat HREE. It is noteworthy that the REE patterns lack any Eu anomaly that would have indicated a growth episode coeval with, or in the stability domain of feldspar. This clearly indicates that feldspar inclusions observed in the crystal are not in equilibrium with garnet. The most striking feature is the variation in HREE as evidenced by the gradual lowering, from core to rim, of the Yb_N/Gd_N ratio, ranging from c. 4.1 to 0.5 respectively. Y, often used as a proxy for HREE mimics this behavior and displays a variation from 250 to 30 ppm. The gradual HREE depletion is attributed to growth zoning rather than diffusion as diffusion coefficient for the trivalent cations are smaller than those for the major divalent cations (Tirone et al., 2005). The influence of mineral

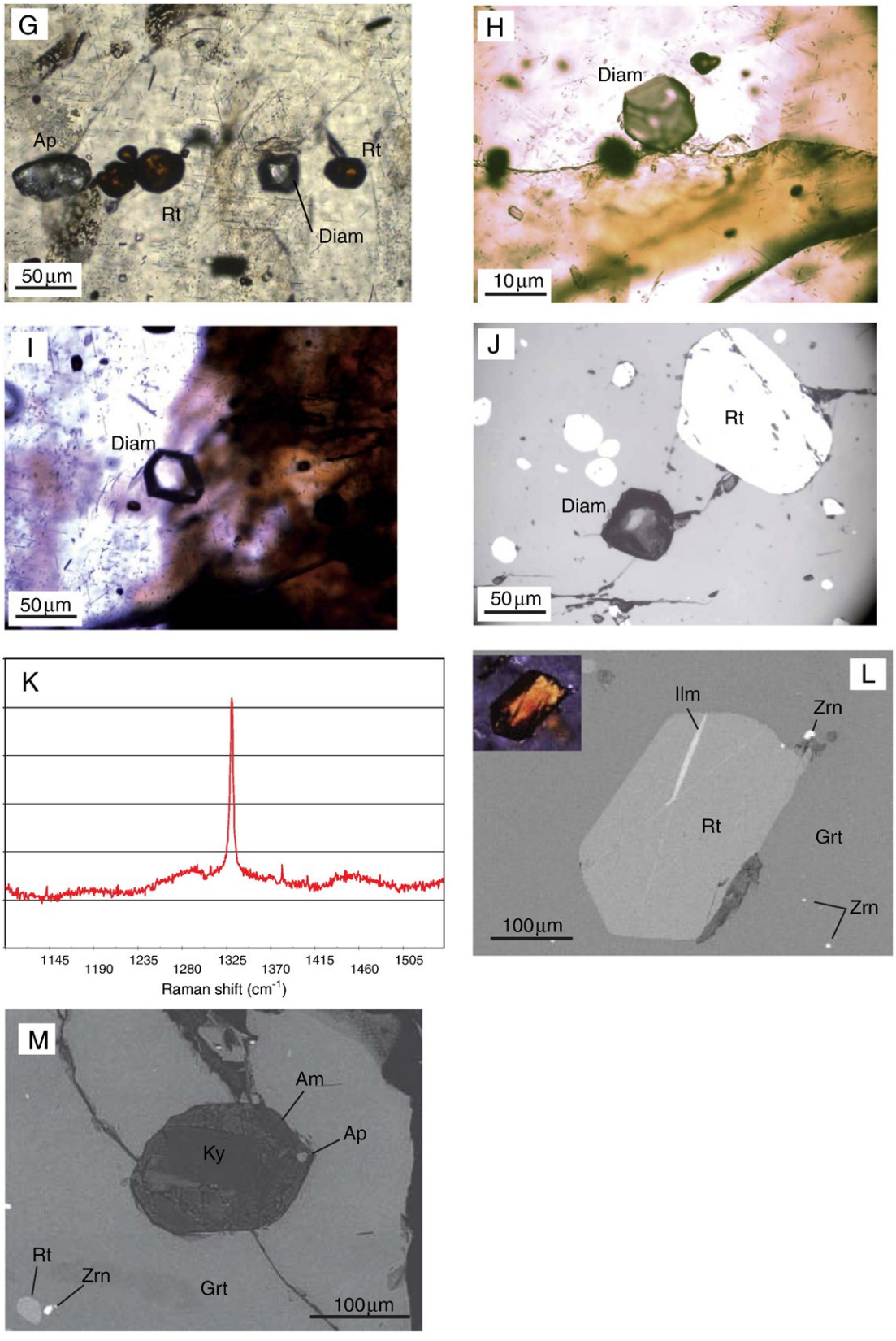

Fig. 3 (*continued*).

breakdown in the reacting rock volume and the liberation of trace elements is not consistent with the observed gradual variations as this would have resulted in abrupt changes in the REE patterns as observed for garnet from UHP eclogite (e.g. Konrad-Schmolke et al., 2008b). The observed zoning is thus likely to reflect crystallization in a closed system, following a process similar to a Rayleigh fractionation mechanism.

Table 1
Major element (wt.% oxide) compositions of selected locations from garnet megacryst ED128 analyzed by electron microprobe. Analyses labeled #1 to #4 refer to locations in Fig. 4. Garnet is normalized on the basis of 12 oxygens and 8 cations. Alm = almandine, Grs = grossular, Pyr = pyrope, Sps = spessartine.

Dataset/point	#1	#2	#3	#4a	#4b
SiO2	38.815	38.764	38.327	38.342	38.714
TiO2	0.163	0.147	0.084	0.072	0.017
Al2O3	22.163	22.367	22.115	21.820	21.914
Cr2O3	0.065	0.089	0.079	0.110	0.046
FeO	25.541	26.143	26.216	26.402	26.934
MnO	0.640	0.805	1.051	1.139	1.215
Mn ppm	4955	6237	8142	8822	9409
MgO	9.087	8.953	8.432	7.864	8.139
CaO	3.993	3.570	3.549	3.841	3.745
Na2O	0.031	0.044	0.043	0.026	0.033
K2O	–	0.004	0.005	0.006	–
P2O5	0.032	0.128	0.091	0.076	0.073
Cl	–	0.005	0.007	0.001	0.008
Total	100.53	101.02	100.00	99.70	100.84
Si	2.962	2.953	2.957	2.976	2.970
Ti	0.009	0.008	0.005	0.004	0.001
Al	1.993	2.008	2.011	1.996	1.981
Cr	0.004	0.005	0.005	0.007	0.003
Fe3+	0.060	0.064	0.061	0.038	0.075
Fe2+	1.570	1.601	1.630	1.676	1.653
Mn	0.041	0.052	0.069	0.075	0.079
Mg	1.034	1.017	0.970	0.910	0.931
Ca	0.326	0.291	0.293	0.319	0.308
Na	0.005	0.007	0.006	0.004	0.005
K		0.000	0.000	0.001	
Alm (mol%)	52.832	54.076	55.033	56.236	55.653
Prp (mol%)	34.790	34.331	32.742	30.533	31.331
Grs (mol%)	10.987	9.838	9.905	10.718	10.360
Sps (mol%)	1.391	1.754	2.319	2.512	2.656

6.2. Rutile

Rutile inclusions in garnet megacryst ED128 are translucent reddish, euhedral with sizes up to 300 μm (Fig. 3L). In back-scattered electron mode, rutile often displays bright bands or domains that correspond to ilmenite exsolution. These bands or domains were avoided during analyses, and all rutile analyses display low (b 3%) iron content (see Table 2). This is in agreement with Fe_2O_3 solubility in rutile (Bromiley et al., 2004) suggesting that increasing amounts of iron can be incorporated in rutile at increasing P, with Fe_2O_3 contents not higher than 3.5% at 5 GPa. Trace element analyses indicate very low level of REE (b 100 ppt), comparable or below the detection limits. This is in agreement with experimentally determined partition coefficients (Klemme et al., 2005) indicating that REEs are incompatible in rutile. On the contrary, HFSE (Zr, Nb, Ta, Hf) have high content along with transition metal elements such as V, Cr and Fe. In the Cr vs Nb diagram (Fig. 6) of Meinhold et al. (2008) or modified after Triebold et al. (2012), rutile grains are tightly grouped and clearly plot in the field of mafic protolith. In the Zr/Hf against Nb/Ta diagram (Fig. 7), all analyzed rutiles display subchondritic Nb/Ta ratios, and subchondritic as well as suprachondritic Zr/Hf ratios. Mean Zr/Hf and Nb/Ta ratios are 34.0 ± 3.4 and 14.7 ± 2.1 (1SD; n = 12) respectively. These values are close to or within uncertainties of the mean Zr/Hf and Nb/Ta ratios of Global MORB (37.5 and 15.5 respectively after Aravelo and McDonough, 2010). In addition, most rutiles plot in, or close to, the MORB field. A MORB protolith for this sample is also in agreement with the coupled substitution $P^{5+} + Na^{+} \rightarrow Si^{4+} + Ca^{2+}$ observed in the inner part of garnet ED128 (Fig. 4B and C). This substitution depends on the Na_2O content of the protolith (Konzett et al., 2012) and is important in MORB type lithologies due to high Na content (2.01 wt.% in average for global MORB after Aravelo and McDonough, 2010). Scattering of some analyses outside of the MORB domain may suggest post-crystallization disturbances, or that a uniform HFS element concentration has not been achieved during prograde metamorphism and the rutile growth (e.g. Meyer et al., 2011).

Several calibrations have been developed for the Zr-in-rutile thermometry (Ferry and Watson, 2007; Tomkins et al., 2007; Watson et al., 2006 and Zack et al., 2004). Among these different calibrations, only the Tomkins' calibration takes P into account and is probably better suited for pressure dominated metamorphism, while other calibrations were empirically (Zack et al., 2004) or experimentally (Ferry and Watson, 2007; Watson et al., 2006) determined for P close to 10 kbars. An important caution to the use of the Zr-in-rutile thermometry is the occurrence of zircon and quartz in the rock during the growth of rutile. In the case of mafic lithologies (such as ED128), silica can be buffered by minerals other than quartz, but the lack of cogenetic zircon results in an underestimation of the metamorphic temperatures (Watson et al., 2006). The temperatures determined in this study are thus minimum values. Rutile from ED128 yields Zr contents ranging from 491 to 272 ppm. Taking into account the occurrence of diamond inclusions in the garnet megacryst ED128, we used the calibration of Tomkins et al. (2007) for the coesite field and a pressure of 3.0 GPa, to calculate a temperature range of 778 to 724 °C and a mean temperature of 750 °C. The calibration of Zack et al. (2004), returns a mean Zr-in-rutile temperature very close at 743 °C, whereas those of Watson et al. (2006) and Ferry and Watson (2007) yield significantly lower temperatures of 658 and 659 °C respectively. The calculated temperatures are within or slightly above the closure temperature for Zr diffusion in rutile (560–730 °C) as defined by Watson et al. (2006) using a grain size of 100 μm and different cooling rates. Given that the investigated rutile grains have larger grain sizes (N 100 μm and up to 300 μm) and are shielded in the garnet, the calculated temperatures are attributed to those prevailing during rutile growth, not to a later cooling.

7. Discussion

7.1. Constraints on UHP metamorphic conditions

The occurrence of diamond inclusions, the index mineral of UHP metamorphism with coesite, in the studied garnet megacryst indicates that the protolith material, at some stage of its evolution, underwent UHP conditions and was buried down to at least 95–120 km depth corresponding to a minimal pressure of c. 2.9–3.0 GPa. However, it was not possible to analyze the bulk-rock, and mineral inclusions in the megacryst do not allow constraining further the metamorphic conditions by means of geothermobarometers. Zr-in-rutile thermometry using the calibration of Tomkins et al. (2007) for the coesite field and a pressure of 3.0 GPa gives a minimum temperature range of 724–778 °C. An independent constraint on temperature is related to the preservation of growth zoning in major and trace elements in the megacryst, suggesting that it did not undergo diffusion reequilibration at elevated temperatures. Spear (1991) indicates that major element zonation in garnet can be reset at temperatures higher than 650 °C. This is in agreement with experimental data on REE (Tirone et al., 2005), which indicates a closure temperature for Sm-Nd of 660 °C for cooling rates of about 2 °C/Ma and a grain size of 3 mm. Results from both studies contrast with the range of temperature given by the Zr-in-rutile thermometer (724–778 °C), that is in excess of the diffusivities for major and rare earth elements in garnet. The preservation of zoning in the megacryst thus implies that the studied garnet either did not reside at such high temperatures for a long time, or more likely that the large grain size of the megacryst (pluricentimetric) significantly lowered the diffusion coefficient for major and rare earth elements if the grain size is taken as the effective diffusion radius. Combining the mean Zr-in-rutile temperature of 750 °C with the new graphite-diamond equilibrium curve of Day (2012) results in a pressure estimate of 3.6 GPa for entering the diamond stability field. In the light of the present data it is thus tentatively proposed that P–T conditions as deduced from the occurrence of diamond and Zr-in-rutile thermometry are T of c. 750 °C and P of 3.6 GPa. At first sight, it is tempting to interpret these P–T conditions as reflecting the peak of UHP metamorphism.

Table 2
Trace element (ppm) compositions of the garnet megacryst ED128 and its rutile inclusions analyzed by laser ablation ICP-MS. Garnet analyses are reported from core (#Gt_1) to rim (#Gt_31) and follow the traverse through the megacryst shown in Fig. 4. Concentrations have been calculated using Si and Ti as internal standards for garnet and rutile respectively. W = Watson et al., 2006; FW = Ferry and Watson, 2007; Z = Zack et al., 2004; T = Tomkins et al., 2007.

Element	Si	P	Ca	Sc	Ti	V	Cr	Mn	Fe	Co	Ni	Rb	Sr	Y	Zr	Nb	Mo	Ba	La	Ce	Pr	Nd	Sm
ED128 Garnet megacryst																							
Rutile																							
#Rt1		7.7		17.4	576,187	1299	1512		5827	0.029			2.0	0.17	419	149	1.0						0.017
#Rt2	36	12.4		18.1	576,187	1301	1286		6252				2.0	0.33	491	144	1.0		0.018	0.008	0.004	0.003	0.022
#Rt3		5.2		9.2	576,187	1382	1431	1.6	13,158	0.33		0.005	1.9	0.40	418	135	1.2		0.000	0.039	0.010	0.037	0.038
#Rt4		5.8		9.4	576,187	1363	1304		7679				1.7	0.13	366	135	0.8		0.001		0.002	0.002	
#Rt5	121	12.4		9.8	576,187	1418	1396	2.9	20,657	0.142			1.8	0.11	373	131	1.5	0.013	0.003			0.017	0.028
#Rt6	29	10.4		9.4	576,187	1389	1339	0.4	16,453			0.022	1.8	0.12	396	132	1.0			0.005		0.011	0.002
#Rt7		1.9		8.8	576,187	1385	1301	0.2	17,533	0.037			1.6	0.12	350	126	0.9					0.006	
#Rt8	24	5.9		8.0	576,187	1383	1236	0.3	7546	0.061			1.7	0.16	356	126	0.9	0.034	0.010	0.008	0.005	0.028	0.013
#Rt9		1.8	1.4	7.2	576,188	1490	1354		6591				1.5	0.10	341	107	0.9				0.003	0.034	0.019
#Rt10	1022	11.3		7.1	576,188	1505	1352		6170			0.002	1.5	0.12	337	108	0.9					0.004	0.006
#Rt11		2.3		8.9	576,188	1762	1450		18,755				1.5	0.13	281	108	0.7		0.055	0.004	0.005	0.015	0.014
#Rt12		2.8		8.8	576,188	1670	1321		6656	0.018		0.001	1.4	0.13	272	104	0.6					0.015	0.019
Garnet																							
#Gt_1	180,385	530	22,498	147	615	80	390	8695	302,704	33				238	30.2	0.017	0.44		0.002	0.006	0.005	0.47	2.1
#Gt_2	180,385	528	23,130	151	600	79	372	8399	234,830	32	2.4	0.04	0.02	229	28.1	0.018	0.29		0.006	0.029	0.015	0.39	2.0
#Gt_3	180,385	531	22,272	142	556	76	359	8228	238,273	31	2.3	0.05	0.06	228	29.5	0.007	0.42	0.005	0.006	0.022	0.014	0.49	2.1
#Gt_4	180,385	467	23,832	153	548	90	418	8760	243,197	32	1.5	0.03	0.05	229	26.3	0.004	0.39		0.004	0.024	0.019	0.49	2.0
#Gt_5	180,385	344	24,501	157	700	98	396	8654	239,988	32	2.0	0.09	1.04	250	22.3	0.042	0.45	0.039	0.015	0.048	0.017	0.43	1.9
#Gt_6	180,385	496	23,160	145	808	80	315	8646	245,349	32	1.8	0.04	0.06	238	29.6	0.006	0.47		0.005	0.030	0.014	0.56	2.3
#Gt_7	180,385	412	24,362	142	1062	93	318	8424	243,781	32	1.7	0.05	0.06	246	30.1	0.002	0.40		0.001	0.016	0.019	0.85	2.8
#Gt_8	180,385	393	25,185	161	1223	90	366	8648	240,163	32	2.1	0.06	0.07	247	27.1	0.014	0.31		0.007	0.036	0.022	0.59	2.3
#Gt_9	180,385	466	25,122	139	971	90	344	8736	245,765	32	2.4	0.06	0.06	243	28.5	0.024	0.27		0.005	0.021	0.018	0.67	2.5
#Gt_10	180,385	420	24,027	118	774	92	328	8363	248,519	32	2.2	0.06	0.05	214	29.9	0.004	0.51	0.025	0.001	0.020	0.017	0.84	2.6
#Gt_11	180,385	401	25,113	122	867	103	343	8442	249,696	33	2.0	0.03	0.06	199	29.0	0.014	0.33	0.026	0.001	0.020	0.021	0.73	2.7
#Gt_12	180,385	456	23,402	123	878	94	347	8034	247,560	33	1.7	0.09	0.04	176	29.6	0.025	0.35			0.007	0.016	0.67	2.5
#Gt_13	180,385	466	21,456	111	651	95	335	7327	248,078	30	2.2	0.06	0.05	150	30.6	0.004	0.27			0.021	0.017	0.57	2.3
#Gt_14	180,385	392	25,164	114	668	114	428	7782	256,804	34	2.1	0.04	0.06	152	26.4	0.009	0.40		0.005	0.027	0.015	0.60	2.5
#Gt_15	180,385	493	24,388	90	767	109	381	7403	249,653	34	2.8	0.03	0.04	116	29.8	0.009	0.19		0.000	0.010	0.024	0.75	2.6
#Gt_16	180,385	414	22,483	93	666	119	417	6821	250,218	34	2.7	0.02	0.04	96	27.7	0.012	0.38			0.009	0.016	0.59	2.4
#Gt_17	180,385	414	24,018	89	1250	140	483	6678	249,683	34	2.3	0.05	0.14	97	28.1	0.006	0.52	0.010	0.002	0.026	0.027	0.89	3.0
#Gt_18	180,385	494	22,195	97	907	124	446	6566	248,349	35	2.6	0.05	0.06	97	30.6	0.005	0.52		0.001	0.025	0.031	0.86	2.9
#Gt_19	180,385	300	28,915	119	782	175	610	6386	243,384	33	2.3	0.05	0.07	121	22.7	0.010	0.54		0.001	0.019	0.027	1.08	4.2
#Gt_20	180,385	282	29,170	132	751	182	635	6229	242,458	34	2.9	0.06	0.07	115	22.6	0.009	0.55	0.003	0.001	0.019	0.029	1.06	4.4
#Gt_21	180,385	284	28,796	127	912	183	688	6004	238,095	33	2.5	0.05	0.09	118	22.5	0.006	0.42		0.002	0.024	0.024	0.99	4.2
#Gt_22	180,385	281	29,233	113	666	186	618	5870	238,802	34	2.9	0.03	0.07		21.8	0.006	0.42	0.000	0.001	0.022	0.022	1.03	4.2
#Gt_23	180,385	264	29,283	108	899	190	627	5789	234,981	34	2.6	0.05	0.09	109	21.3	0.015	0.50		0.002	0.031	0.030	1.11	4.1
#Gt_24	180,385	266	28,649	82	801	185	742	5495	229,838	34	2.5	0.04	0.06	93	20.8	0.006	0.56	0.001	0.001	0.026	0.036	1.13	4.0
#Gt_25	180,385	261	28,490	82	686	183	341	5423	230,911	35	2.9	0.04	0.07	91	20.7	0.006	0.50	0.008	0.001	0.022	0.026	0.90	3.6
#Gt_26	180,385	273	28,360	79	756	180	509	5266	227,755	35	2.4	0.03	0.05	88	21.1	0.004	0.53		0.001	0.026	0.040	1.04	3.8
#Gt_27	180,385	250	28,252	37	819	188	889	4954	224,004	35	2.8	0.00	0.07	36	83.0	0.006	0.46	0.002	0.001	0.034	0.042	1.24	4.0
#Gt_28	180,385	245	28,441	42	835	191	891	4951	221,682	35	2.8	0.01	0.06	38	20.3	0.011	0.53		0.009	0.040	0.038	1.11	3.8
#Gt_29	180,385	245	28,604	45	695	193	892	4949	219,150	35	3.4	0.01	0.09	40	19.9	0.012	0.43	0.074	0.016	0.069	0.038	0.99	3.5
#Gt_30	180,385	245	27,939	44	633	186	1034	4812	217,969	35	2.7	0.01	0.09	40	19.3	0.006	0.49		0.008	0.046	0.036	0.94	3.5
#Gt_31	180,385	306	24,701	45	430	176	928	4743	220,569	36	2.6	0.01	0.05	37	23.1	0.009	0.54	0.002	0.006	0.035	0.016	0.49	2.2

Table 2 (*continued*)

Trace element (ppm) compositions of the garnet megacryst ED128 and its rutile inclusions analyzed by laser ablation ICP-MS. Garnet analyses are reported from core (#Gt_1) to rim (#Gt_31) and follow the traverse through the megacryst shown in Fig. 4. Concentrations have been calculated using Si and Ti as internal standards for garnet and rutile respectively. W = Watson et al., 2006; FW = Ferry and Watson, 2007; Z = Zack et al., 2004; T = Tomkins et al., 2007.

Element	Eu	Gd	Tb	Dy	Ho	Er	Tm	Yb	Lu	Hf	Ta	W	Pb	Th	U	Zr/Hf	Nb/Ta	Zr-in-Rutile thermometry				Yb_N/Gd_N	Eu/Eu*
																		W	FW	Z	T		
ED128 Garnet megacryst																							
Rutile																							
#Rt1			0.007		0.000	0.006	0.002	0.003	0.004	12.3	10.0	0.8	0.011	0.0	1.4	34.0	14.9	671	671	762	763		
#Rt2	0.024		0.014	0.007	0.001	0.041	0.008	0.030	0.015	11.6	9.4	0.6	0.028	0.0	1.3	42.2	15.3	684	685	782	778		
#Rt3		0.103	0.012	0.020	0.007	0.085	0.017	0.053		11.2	9.2	1.5	0.037	0.0	1.6	37.4	14.6	670	671	761	763		
#Rt4		0.030	0.002	0.001		0.001		0.008	0.000	10.4	8.7	0.9	0.012	0.0	1.2	35.1	15.5	659	660	744	750		
#Rt5	0.004		0.005	0.010	0.005	0.011		0.015	0.004	10.6	7.4	0.7	0.022	0.0	1.3	35.2	17.7	661	661	747	752		
#Rt6	0.022	0.115	0.006	0.004	0.000	0.007	0.000	0.004		11.5	11.2	2.2	0.026	0.0	1.3	34.5	11.8	666	666	755	758		
#Rt7	0.011		0.004	0.016	0.002	0.002	0.002		0.002	11.3	8.2	0.7		0.0	1.4	31.1	15.3	655	656	739	746		
#Rt8			0.005		0.003	0.006			0.001	10.7	9.1	0.7	0.094		1.3	33.2	13.9	657	657	741	748		
#Rt9		0.043				0.009	0.003	0.027		11.3	6.4	0.7	0.009	0.0	1.3	30.2	16.8	653	654	735	744		
#Rt10		0.057		0.006		0.006	0.001	0.025	0.003	11.2	6.3	0.7	0.044	0.0	1.3	30.2	17.0	652	653	734	743		
#Rt11	0.003			0.001	0.002	0.006		0.007		9.0	8.7	0.5		0.0	1.1	31.1	12.4	637	638	711	727		
#Rt12				0.011	0.001				0.002	8.0	9.6	0.6		0.0	1.2	34.0	10.9	634	636	706	724		
Garnet																							
#Gt_1	1.9	11.8	3.5	33.1	8.3	28.0	4.5	33.4	5.2	0.52	0.011	0.069				58.1						3.49	1.16
#Gt_2	1.5	10.5	3.2	32.2	8.0	27.7	4.4	35.3	5.4	0.42	0.002	0.033	0.036	0.003		67.1						4.16	1.01
#Gt_3	1.7	10.9	3.3	32.3	8.2	26.8	4.4	32.2	5.0	0.39	0.004	0.011	0.050	0.002		75.7						3.65	1.09
#Gt_4	1.8	10.8	3.3	32.6	8.4	27.6	4.5	34.5	5.3	0.35	0.004		0.026		0.001	74.7						3.95	1.17
#Gt_5	1.9	11.1	3.4	33.8	8.9	30.7	5.0	37.7	6.0	0.27	0.005		0.166	0.002	0.002	83.0						4.21	1.23
#Gt_6	1.9	11.8	3.4	34.0	8.5	27.7	4.4	33.2	5.1	0.34	0.000		0.039	0.001	0.001	87.9						3.49	1.09
#Gt_7	2.2	12.9	3.8	35.7	8.6	27.4	4.3	31.4	4.7	0.37	0.004		0.025	0.001		80.5						3.02	1.11
#Gt_8	1.9	11.7	3.6	34.5	8.8	28.9	4.8	36.1	5.5	0.33	0.002	0.012	0.027	0.003	0.003	81.2						3.81	1.14
#Gt_9	2.0	12.3	3.6	34.5	8.5	27.3	4.3	31.1	4.7	0.35		0.018	0.013	0.001	0.001	81.4						3.14	1.11
#Gt_10	2.1	12.6	3.4	31.8	7.3	21.7	3.5	24.5	3.7	0.39	0.000	0.001	0.001			77.2						2.41	1.13
#Gt_11	2.0	12.9	3.4	29.9	6.8	21.0	3.1	21.9	3.1	0.30		0.006	0.005	0.002	0.002	96.6						2.10	1.02
#Gt_12	1.9	10.9	3.0	26.7	6.3	18.7	2.8	19.6	2.8	0.38	0.003	0.016	0.010	0.002	0.000	78.5						2.22	1.13
#Gt_13	1.9	9.5	2.7	23.5	5.4	15.1	2.3	15.8	2.5	0.37	0.001	0.033	0.031		0.001	82.9						2.05	1.22
#Gt_14	2.1	11.2	2.9	24.8	5.4	16.0	2.3	16.3	2.3	0.33			0.024	0.002	0.002	79.8						1.80	1.23
#Gt_15	2.0	10.6	2.6	20.8	4.2	12.1	1.7	12.0	1.4	0.39		0.020		0.002	0.001	75.7						1.40	1.15
#Gt_16	1.8	10.3	2.3	17.6	3.6	10.1	1.5	9.5	1.3	0.38	0.001	0.009		0.001		72.4						1.14	1.12
#Gt_17	1.9	9.3	2.4	17.5	3.6	10.0	1.5	9.6	1.3	0.41	0.001		0.042		0.003	68.8						1.28	1.09
#Gt_18	1.7	9.1	2.4	17.7	3.8	10.7	1.5	10.2	1.4	0.45	0.001	0.004	0.020	0.000	0.001	68.0						1.38	1.04
#Gt_19	2.5	11.8	3.0	21.9	4.5	13.1	2.0	13.7	2.0	0.35	0.001		0.023	0.000	0.001	65.9						1.44	1.06
#Gt_20	2.6	11.8	2.9	21.1	4.4	12.7	2.0	14.0	2.0	0.31	0.001	0.002	0.023	0.000	0.001	72.6						1.47	1.08
#Gt_21	2.4	11.2	2.8	20.8	4.4	13.3	2.0	13.4	1.9	0.32	0.000	0.013	0.024	0.000	0.002	71.4						1.48	1.09
#Gt_22	2.5	10.7	2.6	19.0	3.9	11.1	1.6	11.3	1.6	0.33	0.001	0.010	0.021	0.000	0.000	66.8						1.31	1.14
#Gt_23	2.5	11.0	2.7	20.4	4.1	11.4	1.7	11.4	1.5	0.32		0.003	0.029	0.000	0.002	66.0						1.27	1.11
#Gt_24	2.4	10.6	2.6	18.1	3.4	8.5	1.1	6.4	0.7	0.27	0.000	0.003	0.025	0.000		76.2						0.75	1.15
#Gt_25	2.3	10.2	2.5	17.8	3.4	8.5	1.2	7.1	0.9	0.28	0.001		0.025		0.001	74.0						0.86	1.14
#Gt_26	2.2	10.1	2.4	17.1	3.2	8.3	1.1	6.6	0.8	0.30	0.001	0.004	0.023		0.001	71.1						0.81	1.12
#Gt_27	2.4	7.4	1.3	7.8	1.3	3.0	0.4	2.2	0.2	1.45		0.000	0.024	0.000	0.011	57.3						0.36	1.33
#Gt_28	2.3	7.5	1.4	8.1	1.4	3.5	0.5	2.8	0.4	0.28	0.000	0.004	0.031		0.002	73.6						0.47	1.34
#Gt_29	2.2	7.4	1.4	8.5	1.5	3.7	0.5	3.1	0.4	0.29	0.001		0.058	0.000	0.002	69.9						0.52	1.28
#Gt_30	2.2	7.3	1.4	8.6	1.4	3.1	0.4	2.2	0.3	0.28		0.005	0.035	0.001	0.001	69.1						0.37	1.29
#Gt_31	1.5	5.7	1.2	7.8	1.3	3.0	0.4	2.2	0.2	0.34	0.000	0.015	0.020	0.001	0.000	67.9						0.48	1.26

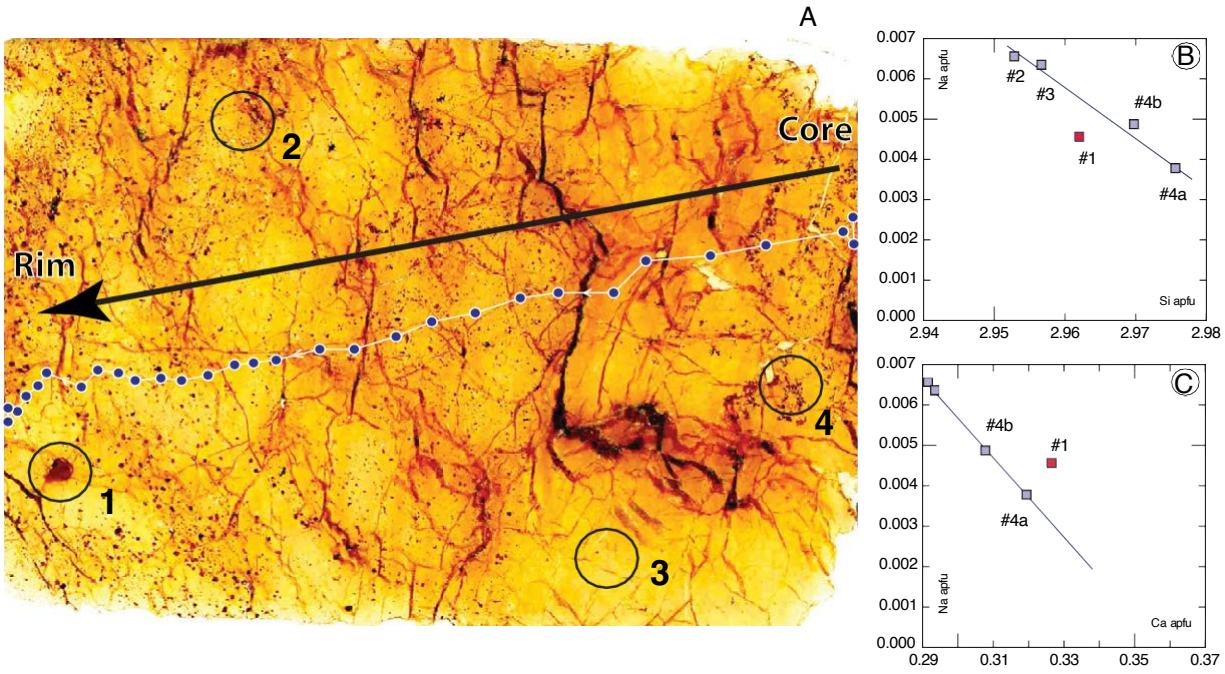

Fig. 4. (A) Thick section of the garnet megacryst ED128 showing the location of the electron microprobe (large circles, labeled 1 to 4) and laser ablation ICP-MS analyses (small circles). Correlation diagrams between Na apfu and Si apfu (B), and Na apfu and Ca apfu (C). The observed correlations, except for the outermost analysis (1), suggest that phosphorus entered the garnet crystal lattice by the coupled substitution $Na^{+} + P^{5+} \rightarrow Si^{4+} + Ca^{2+}$ (Thompson, 1975).

However, recent studies have demonstrated that rutile in UHP lithologies does not necessarily crystallize at peak metamorphism, but can also grow in the prograde path, during subduction of the continental/oceanic crust (Zheng et al., 2011). The P–T estimates quoted above are thus taken as minimum values. In addition, we also note that UHP parageneses have been reported in the Betic-Rif area, and the proposed peak pressure conditions for this material are much higher, in the order of 6–7 GPa (Ruiz-Cruz and Sanz de Galdeano, 2013a,b).

7.2. *Possible geodynamic setting*

Metamorphic diamonds were discovered in a garnet megacryst located in the basal tectonic contact underlying the Kef Lakhal amphibolites of the Edough Massif. According to Bosch et al. (2014), the Kef Lakhal amphibolites represent obducted oceanic arc material that was subjected to dehydration melting conditions at temperatures of 800 °C and pressure of 10–13 kbar (Caby et al., 2001). These P–T values are clearly outside the range of conditions allowing the development of UHP metamorphism and more likely are related to thrusting of the Kef Lakhal unit onto the North African margin. The occurrence of boudins of ultramafic rocks, coarse-grained dunite and actinolite pods indicates that part of the material in the sole represents fragments of mantle origin. This is also consistent with a MORB origin for the protolith of the garnet megacryst as defined by trace elements in rutile. The coexistence of mantle material and high-grade metasedimentary (pelitic) rocks in the sole is consistent with a geodynamical setting in which relics of oceanic lithosphere and adjacent rocks of continental origin were subducted deep down in the stability field of diamond. UHP metamorphic terranes have all been identified in subduction/collisional settings. For example, in the case of the western-central Alps, subduction of Jurassic oceanic crust and mantle from the Piemont-Ligurian oceanic domain took place much earlier (c. 45 Ma after Rubatto and Hermann, 2003) than subduction of continental units (c. 38–35 Ma for Dora

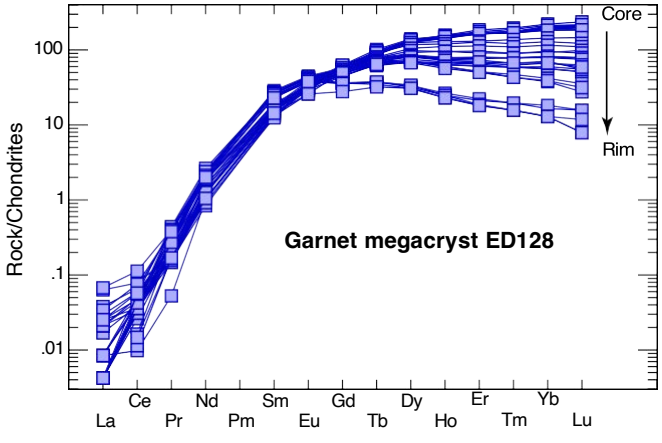

Fig. 5. Chondrite-normalized REE pattern for the garnet megacryst ED128. Normalizing values after Sun and McDonough (1989).

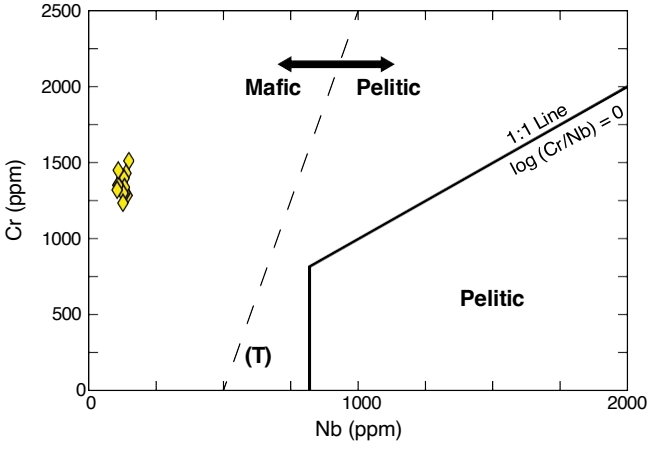

Fig. 6. Cr versus Nb diagram (Meinhold et al., 2008) for prismatic rutile from garnet megacryst ED128. The heavy dashed line is from Triebold et al. (2012) and delimits the field of metamafic and metapelitic rutile.

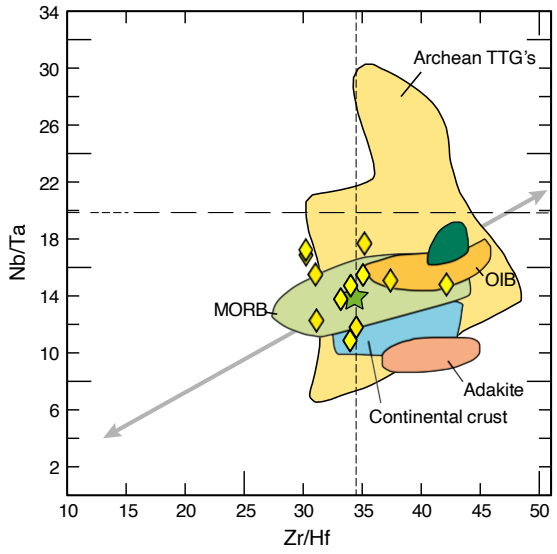

Fig. 7. Zr/Hf against Nb/Ta diagram of Munker et al. (2003), adapted from Meyer et al. (2011) for prismatic rutile from the garnet megacryst ED128. The dashed line corresponds to chondritic values (Zr/Hf = 34.3 and Nb/Ta = 17.5 after McDonough and Sun, 1995). The star is Bulk Silicate Earth. The arrowed line is the silicate differentiation trend.

Maira after Gebauer et al., 1997). In the central Alps, the protoliths of UHP eclogites of Alpe Arami associated with the garnet peridotites are c. 35 Ma old and these were exhumed prior to 32–30 Ma (Gebauer et al., 1997). Most occurrences of metamorphic diamond are known within continental rocks. Occurrences of UHP metamorphic terranes of oceanic affinity are more scarce. This is mainly because oceanic UHP terranes are difficult to exhume since they have higher density than metamorphosed continental terranes, that are positively buoyant until pressures of at least 4 GPa (Massone et al., 2007). Examples of such diamond-bearing UHP units of oceanic affinity include the 100 m thick Lago di Cignana (W. Alps) terrane, a remnant of the Piemontese ocean, tectonically enclosed in the Zermatt-Saas Zone (Reinecke, 1998). The most widely accepted hypothesis for UHP metamorphic rocks to return to shallow depths is related to buoyancy contrast between the subducted rocks. The positive buoyancy of the continental material is responsible for their exhumation via different types of mechanisms (for a review, see Hacker and Gerya, 2013). In the case of the Edough Massif, we propose that the occurrence of UHP units in a mylonite zone, now located between the thrusted Kef Lakhal oceanic unit and the granite-gneiss core would imply a north-dipping subduction of the edge of Africa in order to allow at least part of the granite gneisses to undergo UHP metamorphism. However, UHP rocks have not been reported so far for the continental units of the Edough Massif, although the coexistence of pyrope-rich garnet, kyanite, Zn staurolite and rutile is evidence for very high-pressure metamorphic conditions (Caby et al., 2001). The lack of UHP relics in the dome can also be explained by the fact that it is mostly constituted by diatexites generated at low pressure, with high degree of partial melting estimated at 10–30% after Ahmed-Said and Leake (1995). These high degrees of partial melting may have obliterated the UHP record. The emplacement of the Sidi Mohamed peridotite body at about 18 Ma (Bruguier et al., 2009), to which are linked veins of eclogitized gabbro, is consistent with the fact that part of the basement of the Edough Massif may have been entrained in a subduction zone during the Miocene. Other metamorphic diamond occurrences described in the peri-Mediterranean region include granulites, gneisses and schists from the Betic-Rif Cordillera (Ruiz-Cruz and Sanz de Galdeano, 2013a,b; Ruiz-Cruz et al., 2011), indicating that the UHP metamorphism in the Betic and Rif areas has affected a whole crustal section, conversely to what is presently known for the Edough Massif. In the case of the Betic-Rif Cordillera, as well as in the case of the Edough Massif, the age of the UHP metamorphism is yet to be determined and the precise geodynamical context is unclear. Hidas et al. (2013) recently proposed the inversion of a back-arc basin to explain the crustal emplacement of the Ronda peridotites. A back-arc context was also proposed for the Kef Lakhal oceanic units (Bosch et al., 2014), thrusted onto the North African margin. It is also noteworthy that although the peridotite bodies in the Betic-Rif and in the Tell may have a common origin, as proposed by Hidas et al. (2013), their emplacement in the continental crust occurred at different times. The Ronda and Beni Bousera peridotites were emplaced at 21–23 Ma (Esteban et al., 2011; Zindler et al., 1983), whereas the Edough peridotites were emplaced later, at 18 Ma (Bruguier et al., 2009). These differences potentially point to different contexts and timings that can be best accounted for by the segmentation of an originally single, NW dipping, slab and the individualisation of segments affected by displacements/rotations with different senses, directions and rates (van Hinsbergen et al., 2014). In any case, a global scenario has to take into account i/the early Oligocene age of the collision of Africa with the Lesser and Greater Kabylia, ii/the southeast-directed vergence of the crystalline (Lesser Kabylia) and passive margin sedimentary (Tellian) nappes that were transported on top of the African passive margin and, iii/the Cenozoic evolution of the Western Mediterranean, that is dominated by the eastward retreat of the Calabrian branch of the Tethyan slab inducing opening of basins younging eastward (Carminatti et al., 2012; Doglioni et al., 1997; Faccenna et al., 2001). In the light of the present knowledge, a more plausible scenario to explain the exhumation of UHP units identified in the Edough Massif is related to slab tear or the creation of a slab window affecting the retreating Calabrian branch of the Tethyan slab. Asthenospheric upwelling through the void dragged upward fragments of the UHP (diamond-bearing) Tethyan slab and metasediments and disrupted the Liguro-Provençal basin lithosphere. In this hypothesis, the Kef Lakhal oceanic unit may represent tectonic slices derived from the southern termination of the Liguro-Provençal basin that were pushed onto the North African margin during the onset of opening of the Algerian basin. This scenario is consistent with a model of exhumation related to a trans-mantle diapir, that involves mixing of domains of different pressures in a mélange zone, domal structure and concurrent magmatism (see Table 1 of Hacker and Gerya, 2013).

8. Conclusions

A garnet megacryst from the basal tectonic contact of the Kef Lakhal oceanic unit (Edough Massif, NE Algeria) contains metamorphic diamonds, demonstrating the occurrence of UHP metamorphic rocks until now not recognized in this part of the Western Mediterranean area. Trace elements in rutile indicate that the protolith was of mafic origin, with a MORB affinity. Zr-in-rutile thermometry, combined with the graphite–diamond equilibrium curve indicates UHP metamorphic conditions of at least 750 °C and 3.6 GPa. We suggest that the mafic protolith represents slices of the retreating Calabrian branch of the Tethyan slab, that broke or tore, thus allowing the rise of a mantle flow. Fragments of UHP material were dragged upward by this mantle flow, thrusted onto the deeply buried North African margin together with arc crust, prior to the extensional period when the Algerian basin started opening and the Edough core complex was exhumed, followed by the extrusion of the Langhian rhyolitic lavas.

Acknowledgments

We are grateful to C. Nevado and D. Delmas who provided high quality polished thin sections, to B. Boyer for electron microprobe analyses, to F. Fernandez for SEM imaging and to J.M. Ruiz for Raman spectrocopy. This work has benefited from a financial support of the 2013 and 2014 SYSTER program from the Institut National des Sciences de l'Univers-Centre National de la Recherche Scientifique (INSU-CNRS,

France) to D.B. (title: Opening of the Western Mediterranean: Insights from the orogenic peridotites of NE Algeria). We also thank the CNRS/DPGRF Program for a grant (N°52859), which allowed exchanges between French and Algerian researchers. This study is part of the PhD work of L.F., financially supported by a grant from the French Research Ministry. The authors are grateful to Guillermo Booth Rea and to Dominique Frizon de Lamotte whose comments significantly helped us improve this manuscript.

References

Ahmed-Said, Y., Leake, B.E., 1992. The composition and origin of Kef Lakhal amphibolites and associated amphibolite and olivine-rich enclaves, Edough, Annaba, NE Algeria. Min. Mag. 56, 459–468.

Ahmed-Said, Y., Leake, B.E., 1995. The petrogenesis of the Edough orthogneisses, Annaba, northeast Algeria. J. Afr. Earth Sci. 21, 253–269.

Ahmed-Said, Y., Leake, B.E., 1997. The petrogenesis of the Edough amphibolites, Annaba, NE Algeria; two unrelated basic magmas and the lherzolite–harzburgite residue of a possible magma source. Mineral. Petrol. 59, 207–237.

Aravelo, R., McDonough, W.F., 2010. Chemical variations and regional diversity observed in MORB. Chem. Geol. 271, 70–85.

Block, L., Royden, L.H., 1990. Core complex geometries and regional scale-flow in the lower crust. Tectonics 9, 557–567.

Bosch, D., Hammor, D., Mechati, M., Fernandez, L., Bruguier, O., Caby, R., Verdoux, P., 2014. Geochemical study (major, trace elements and Pb–Sr–Nd isotopes) of mantle material obducted onto the North African margin (Edough Massif, North Eastern Algeria): Tethys fragments or lost remnants of the Liguro-Provençal basin? Tectonophysics 626, 53–68.

Bossière, G., Collomb, P., Mahdjoub, Y., 1976. Sur un gisement de péridotite découvert dans le massif de l'Edough (Annaba, Algérie). C. R. Acad. Sci. Paris série II, 1039–1045.

Bouillin, J.-P., Durand Delga, M., Olivier, P., 1986. Betic-Rif and Tyrrhenian: distinctive features, genesis and development stages. In: Wezel, F.C. (Ed.), The Origin of Arcs. Elsevier, Amsterdam, pp. 281–304.

Bromiley, G., Hilaret, N., McCammon, C., 2004. Solubility of hydrogen and ferric iron in rutile and TiO2 (II): implications for phase assemblages during ultrahigh-pressure metamorphism and for the stability of silica polymorphs in the lower mantle. Geophys. Res. Lett. 31. http://dx.doi.org/10.1029/2004GL019430 (L04610).

Bruguier, O., Hammor, D., Bosch, D., Caby, R., 2009. Miocene incorporation of peridotite into the Hercynian basement of the Maghrebides (Edough Massif, NE Algeria): implications for the geodynamic evolution of the Western Mediterranean. Chem. Geol. 261, 171–183.

Brun, J.P., Van Den Driessche, J., 1994. Extensional gneiss domes and detachment fault systems: structure and kinematics. Bull. Soc. Geol. Fr. 165, 519–530.

Brunel, M., Hammor, D., Misseri, M., Gleizes, G., Bouloton, J., 1988. Cisaillements synmétamorphes avec transport vers le Nord-Ouest dans le massif cristallin de l'Edough (Wilaya d'Annaba, Algérie): Une faille normale ductile hercynienne? C. R. Acad. Sci. Paris 306, 1039–1045.

Caby, R., Hammor, D., 1992. Le massif de l'Edough (Algérie): Un "Metamorphic Core Complex" d'âge miocène dans les Maghrébides. C. R. Acad. Sci. Paris 314, 29–835.

Caby, R., Hammor, D., Delor, C., 2001. Metamorphic evolution, partial melting and Miocene exhumation of lower crust in the Edough metamorphic core complex, west Mediterranean orogen, Eastern Algeria. Tectonophysics 342, 239–273.

Carminatti, E., Lustrino, M., Doglioni, C., 2012. Geodynamic evolution of the Central and Western Mediterranean: tectonics vs igneous petrology constraints. Tectonophysics 579, 173–192.

Cheilletz, A., Ruffet, G., Marignac, C., Kolli, O., Gasquet, D., Féraud, G., 1999. $^{40}Ar/^{39}Ar$ dating of shear zones in the Variscan basement of Greater Kabylia (Algeria). Evidence for an Eo-Alpine event at 128 Ma (Hauterivian-Barremian boundary): geodynamic consequences. Tectonophysics 306, 97–116.

Chopin, C., 2003. Ultrahigh-pressure metamorphism: tracing continental crust into the mantle. Earth Planet. Sci. Lett. 212, 1–14.

Davis, G.H., 1987. A shear zone model for the structural evolution of metamorphic core complexes in southeastern Arizona. In: Coward, M.P., Dewey, J.F., Hancock, P.L. (Eds.), Continental Extensional Tectonics. Spec. Pub. Geol. Soc. London 28, pp. 247–266.

Day, H.W., 2012. A revised diamond–graphite transition curve. Am. Mineral. 97, 52–62.

Dobrzhinetskaya, L.F., 2012. Microdiamonds — frontier of ultrahigh-pressure metamorphism: a review. Gondwana Res. 21, 207–223.

Doglioni, C., Gueguen, E., Sabat, F., Fernandez, M., 1997. The western Mediterranean extensional basins and the Alpine orogeny. Terra Nova 9, 109–112.

Esteban, J.J., Cuevas, J., Tubia, J.M., Sergeev, S., Larionov, A., 2011. A revised Aquitanian age for the emplacement of the Ronda peridotites (Betic Cordilleras, southern Spain). Geol. Mag. 148, 183–187.

Faccenna, C., Funiciello, F., Giardini, D., Lucente, P., 2001. Episodic back-arc extension during restricted mantle convection in the Central Mediterranean. Earth Planet. Sci. Lett. 187, 105–116.

Ferry, J.M., Watson, E.B., 2007. New thermodynamic models and revised calibrations for the Ti-in-zircon and Zr-in-rutile thermometers. Contrib. Mineral. Petrol. 154, 429–437.

Frizon de Lamotte, D., Saint Bezar, B., Bracène, R., Mercier, E., 2000. The two main steps of the Atlas building and geodynamics of the western Mediterranean. Tectonics 19, 740–761.

Gautier, P., Brun, J.P., 1994. Crustal-scale geometry and kinematics of late-orogenic extension in the central Aegean (Cyclades and Evvia Island). Tectonophysics 238, 399–424.

Gebauer, D., Schertl, H.P., Brix, M., Schreyer, W., 1997. 35 Ma old ultrahigh-pressure metamorphism and evidence for very rapid exhumation in the Dora Maira massif, Western Alps. Lithos 41, 5–24.

Gilotti, J.A., 2013. The realm of ultrahigh-pressure metamorphism. Elements 9, 255–260.

Gleizes, G., Bouloton, J., Bossière, G., Collomb, P., 1988. Données lithologiques et pétro-structurales nouvelles sur le massif cristallophyllien de l'Edough (Est- Algérie). C. R. Acad. Sci. Paris 306, 1001–1008.

Hacker, B.R., Gerya, T.V., 2013. Paradigms, new and old, for ultrahigh-pressure tectonism. Tectonophysics 603, 79–88.

Hadj-Zobir, S., Oberhansli, R., 2013. The Sidi Mohamed peridotites (Edough Massif, NE Algeria): evidence for an upper mantle origin. J. Earth Syst. Sci. 122, 1455–1465.

Hammor, D., Bosch, D., Caby, R., Bruguier, O., 2006. A two-stage exhumation of the Variscan crust: U–Pb LA-ICP-MS and Rb–Sr ages from Greater Kabylia, Maghrebides. Terra Nova 18, 299–307.

Hidas, K., Booth-Rea, G., Garrido, C.J., Martinez-Martinez, J.M., Padron-Navarta, J.A., Konc, Z., Giaconia, F., Frets, E., Marchesi, C., 2013. Backarc basin inversion and subcontinental mantle emplacement in the crust: kilometer-scale folding and shearing at the base of the proto-Alboran lithospheric mantle (Betic Cordillera, southern Spain). J. Geol. Soc. Lond. 170, 47–55.

Klemme, S., Prowatke, S., Mametner, K., Gunther, D., 2005. Partitioning of trace elements between rutile and silicate melts: implications for subduction zones. Geochim. Cosmochim. Acta 69, 2361–2371.

Konrad-Schmolke, M., O'Brien, P.J., de Capitani, C., Carswell, D.A., 2008a. Garnet growth at high- and ultra-high pressure conditions and the effect of element fractionation on mineral modes and composition. Lithos 103, 309–332.

Konrad-Schmolke, M., Zack, T., O'Brien, P.J., Jacob, D.E., 2008b. Combined thermodynamic and rare earth element modeling of garnet growth during subduction: examples from ultrahigh-pressure eclogite of the Western Gneiss Region, Norway. Earth Planet. Sci. Lett. 272, 488–498.

Konzett, J., Dieter Rhede, D., Frost, D.J., 2012. The high PT stability of apatite and Cl partitioning between apatite and hydrous potassic phases in peridotite: an experimental study to 19 GPa with implications for the transport of P, Cl and K in the upper mantle. Contrib. Mineral. Petrol. 163, 277–296.

Kretz, R., 1983. Symbols for rock forming minerals. Am. Mineral. 68, 277–279.

Liou, J.G., Ernst, W.G., Zhang, R.Y., Tsujimori, T., Jahn, B.M., 2009. Ultrahigh-pressure minerals and metamorphic terranes — the view from China. J. Asian Earth Sci. 35, 199–231.

Lister, G.S., Davis, G.A., 1989. The origin of metamorphic core complexes and detachment faults formed during tertiary extension in the northern Colorado River region, U.S.A. J. Struct. Geol. 11, 65–94.

Mahdjoub, Y., Choukroune, P., Kiénast, J.R., 1997. Kinematics of a complex Alpine segment: surimposed tectonic and metamorphic events in the Petite Kabylie Massif (northern Algeria). Bull. Soc. Geol. Fr. 168, 649–661.

Massone, H.J., Willner, A.P., Gerya, T.V., 2007. Densities of metapelitic rocks at high to ultrahigh pressure conditions: what are the geodynamic consequences. Earth Planet. Sci. Lett. 256, 12–27.

McDonough, W.F., Sun, S.S., 1995. The composition of the Earth. Chem. Geol. 120, 223–253.

Meinhold, G., Anders, B., Kostopoulos, D., Reischmann, T., 2008. Rutile chemistry and thermometry as provenance indicator: an example from Chios Island, Greece. Sediment. Geol. 203, 98–111.

Meyer, M., John, T., Brandt, S., Klemd, R., 2011. Trace element composition of rutile and the application of Zr-in-rutile thermometry to UHT metamorphism (Epupa Complex, NW Namibia). Lithos 126, 388–401.

Michard, A., 2006. Extension in Alpine Western Europe and West Mediterranean. C. R. Geosci. 338, 225–228.

Michard, A., Negro, F., Saddiqi, O., Bouybaouene, M.L., Chalouan, A., Montigny, R., Goffé, B., 2006. Pressure–temperature–time constraints on the Maghrebide mountain building: evidence from the Rif-Betic transect (Morocco, Spain), Algerian correlations and geodynamic implications. C. R. Geosci. 338, 92–114.

Monié, P., Maluski, H., Saadallah, A., Caby, R., 1988. New $^{40}Ar/^{39}Ar$ ages of Hercynien and alpine thermotectonic events in Grande Kabylie (Algeria). Tectonophysics 152, 53–69.

Mposkos, E.D., Kostopoulos, D.K., 2001. Diamond, former coesite and supersilicic garnet in metasedimentary rocks from the Greek Rhodope: a new ultrahigh-pressure metamorphic province established. Earth Planet. Sci. Lett. 192, 497–506.

Munker, C., Pfander, J.A., Weyer, S., Buchl, A., Kleine, T., Mezger, K., 2003. Evolution of planetary cores and the Earth–Moon system from Nb/Ta systematic. Science 301, 84–87.

Pearce, N.J.G., Perkins, W.T., Westgate, J.A., Gorton, M.P., Jackson, S.E., Neal, C.R., Chenery, S.P., 1997. A compilation of new and published major and trace data for NIST SRM 610 and NIST SRM 612 glass reference materials. Geostand. Newslett. 20, 247–261.

Peucat, J.J., Mahdjoub, Y., Drareni, A., 1996. U–Pb and Rb–Sr geochronological evidence for late Hercynian tectonic and Alpine overthrusting in Kabylian metamorphic basement massifs (northern Algeria). Tectonophysics 258, 195–213.

Reinecke, T., 1998. Prograde high- to ultrahigh-pressure metamorphism and exhumation of oceanic sediments at Lago di Cignana, Zermatt-Saas Zone, Western Alps. Lithos 42, 147–189.

Rubatto, D., Hermann, J., 2003. Zircon formation during fluid circulation in eclogites (Monviso, Western Alps): implications for Zr and Hf budget in subduction zones. Geochim. Cosmochim. Acta 67, 2173–2187.

Ruiz-Cruz, M.D., Sanz de Galdeano, C., 2013a. Coesite and diamond inclusions, exsolution microstructures and chemical patterns in ultrahigh pressure garnet from Ceuta (Northern Rif, Spain). Lithos 177, 184–206.

Ruiz-Cruz, M.D., Sanz de Galdeano, C., 2013b. Diamond and coesite in ultrahigh-pressure–ultrahigh-temperatures granulites from Ceuta, Northern Rif, northwest Africa. Min. Mag. 76, 683–705.

Ruiz-Cruz, M.D., Sanz de Galdeano, C., Garrido, C.J., 2011. Petrology of microdiamond-bearing schists from the Torrox unit, Betic Cordillera, Spain. Econ. Geol. 1241–1249.

Saadallah, A., Caby, R., 1996. Alpine extensional detachment tectonics in the Grande Kabylie metamorphic core complex of the Maghrebides (northern Algeria). Tectonophysics 267, 257–273.

Shertl, H.P., O'Brien, P.J., 2013. Continental crust at mantle depths: key minerals and microstructure. Elements 261–266.

Spear, F.S., 1991. On the interpretation of peak metamorphic temperatures in light of garnet diffusion during cooling. J. Metamorph. Geol. 9, 379–388.

Sun, S.S., McDonough, W.F., 1989. Chemical and isotopic systematics of oceanic basalts: implications for mantle composition and processes. In: Saunders, A.D., Norry, M.J. (Eds.), Magmatism in the Ocean BasinsGeol. Soc. Lond. Blackwells for the Geological Society, London, Oxford, pp. 313–345.

Thompson, R.N., 1975. Is upper mantle phosphorus contained in sodic garnet. Earth Planet. Sci. Lett. 26, 417–424.

Tirone, M., Ganguly, J., Dohmen, R., Langenhorst, F., Hervig, R., Becker, H.W., 2005. Rare earth diffusion kinetics in garnet: experimental studies and applications. Geochim. Cosmochim. Acta 69, 2385–2398.

Tomkins, H.S., Powell, R., Ellis, D.J., 2007. The pressure dependence of the zirconium-in-rutile thermometer. J. Metamorph. Geol. 25, 703–713.

Triebold, S., von Eynatten, H., Zack, T., 2012. A recipe for the use of rutile in sedimentary provenance analysis. Sediment. Geol. 282, 268–275.

Van Hinsbergen, D.J.J., Vissers, R.L.M., Spakman, W., 2014. Origin and consequences of western Mediterranean subduction, rollback and slab segmentation. Tectonics 33. http://dx.doi.org/10.1002/tect.20125.

Vila, J., 1970. Le Djebel Edough: un massif cristallin externe du Nord-Est de la Berbérie. Bull. Soc. Geol. Fr. 12, 805–812.

Watson, E.B., Wark, D.A., Thomas, J.B., 2006. Crystallisation thermometers for zircon and rutile. Contrib. Mineral. Petrol. 151, 413–433.

Zack, T., Moraes, R., Kronz, A., 2004. Temperature dependence of Zr in rutile: empirical calibration of a rutile thermometer. Contrib. Mineral. Petrol. 148, 471–488.

Zheng, Y.-F., Gao, X.-Y., Chen, R.-X., Gao, T., 2011. Zr-in-rutile thermometry of eclogite in the Dabie orogeny: constraints on rutile growth during continental subduction-zone metamorphism. J. Asian Earth Sci. 40, 427–451.

Zindler, A., Staudigel, H., Hart, S.R., Endres, R., Goldstein, S., 1983. Nd and Sm isotopic study of a mafic layer from Ronda ultramafic complex. Nature 304, 226–228.